Supplement of Atmos. Meas. Tech., 18, 4573–4591, 2025
https://doi.org/10.5194/amt-18-4573-2025-supplement

Atmospheric Measurement Techniques
Open Access
EGU

Supplement of

Real-time organic aerosol characterization via Orbitrap mass spectrometry in urban and agricultural environments

Julia David et al.

Correspondence to: Julia David (david@iau.uni-frankfurt.de) and Alexander L. Vogel (vogel@iau.uni-frankfurt.de)

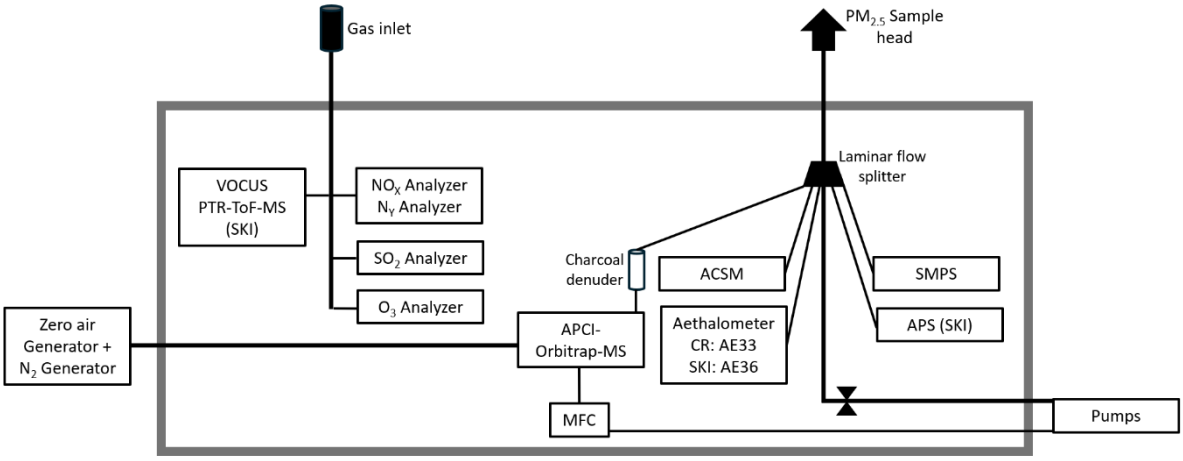

Figure S1: Schematic of the mobile laboratory container setup (not to scale). The container (4.5 m x 1.4 m x 2.3 m, L x D x H) was equipped with an air conditioning unit to maintain temperatures between 20 °C and 24 °C. External equipment included a compressor for the zero-air and nitrogen generator (for Orbitrap calibration), pumps for the particle inlet system, SMPS, and gas monitors. Gas-phase instruments included NO_x, N_Y, SO_2 and O_3 analysers and in SKI a PTR-ToF-MS. Particle-phase measurements were conducted using a $PM_{2.5}$ inlet with regulated airflow. A laminar flow splitter distributed aerosol flow to the SMPS, ACSM, Aethalometer (CR: AE33, SKI: AE36s), APS (SKI), and APCI-Orbitrap-MS. To ensure only particle-phase measurements, the aerosol flow passed through a charcoal denuder, with airflow regulated at 1.6 L min^{-1} by an MFC and pump.

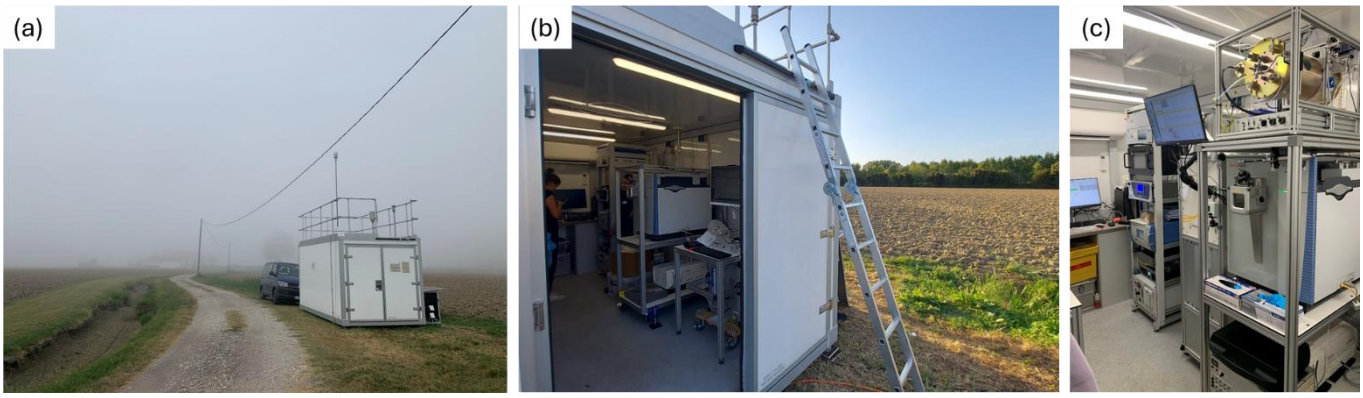

Figure S2: Pictures of the mobile laboratory container in SKI. a) shows agricultural surrounding on a foggy day; b) closer picture showing the APCI-Orbitrap-MS and ACSM as well as agricultural field next to it; c) closeup of the APCI-Orbitrap-MS, VOCUS PTR-ToF-MS and gas monitors (NO_X, N_Y, SO_2, O_3).

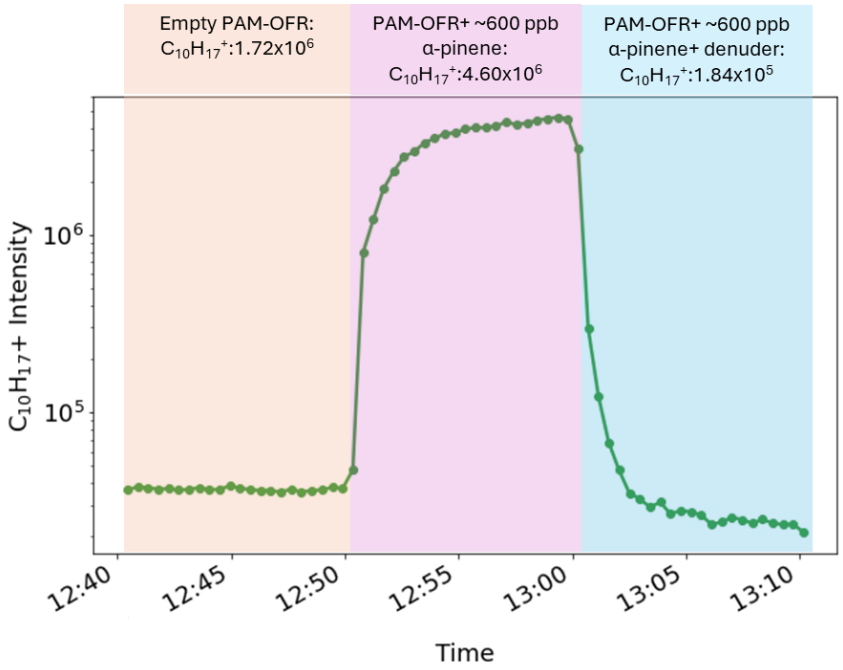

Figure S3: Denuder efficiency test showing $C_{10}H_{17}^+$ intensity over time for an empty PAM-OFR (orange), ~600 ppb α-pinene in PAM-OFR (purple), and ~600 ppb α-pinene after charcoal denuder (blue).

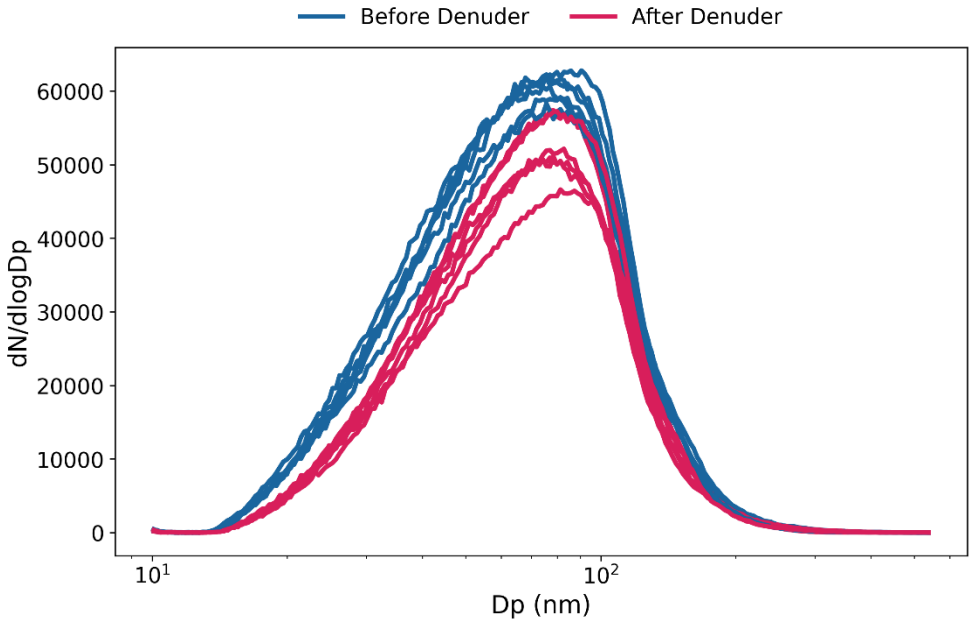

Figure S4: Denuder transmission efficiencies from α-pinene PAM-OFR experiments before (blue) and after (red) the charcoal denuder for size dependent losses, shown as the dN/dlogDp [1 cm^{-3}] over the particle size [nm] range.

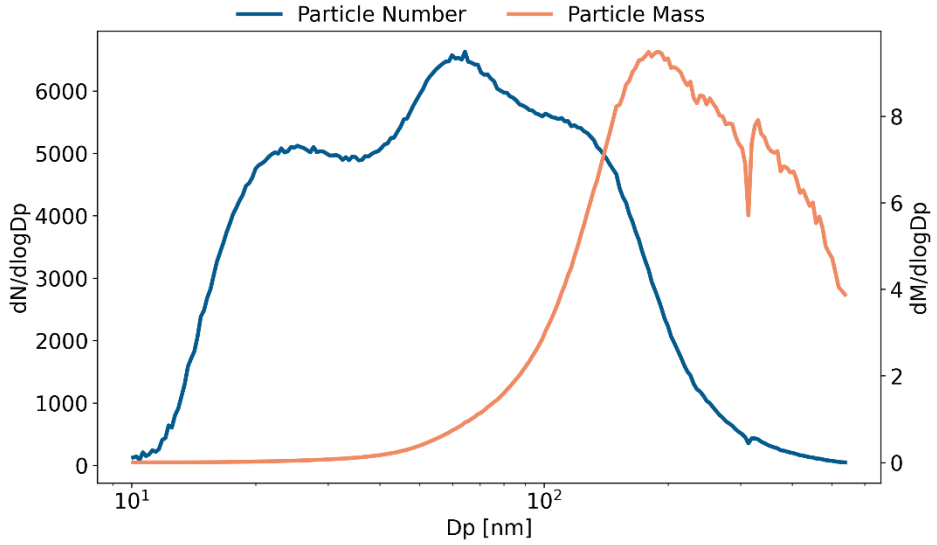

Figure S5: SMPS measurements from CR between 07. July and 10. July 2023. Shown are the particle number dN/dlogDp [1/cm^{-3}] in blue and particle mass dM/dlogDp [µg/m^{-3}] in orange over the measured size range.

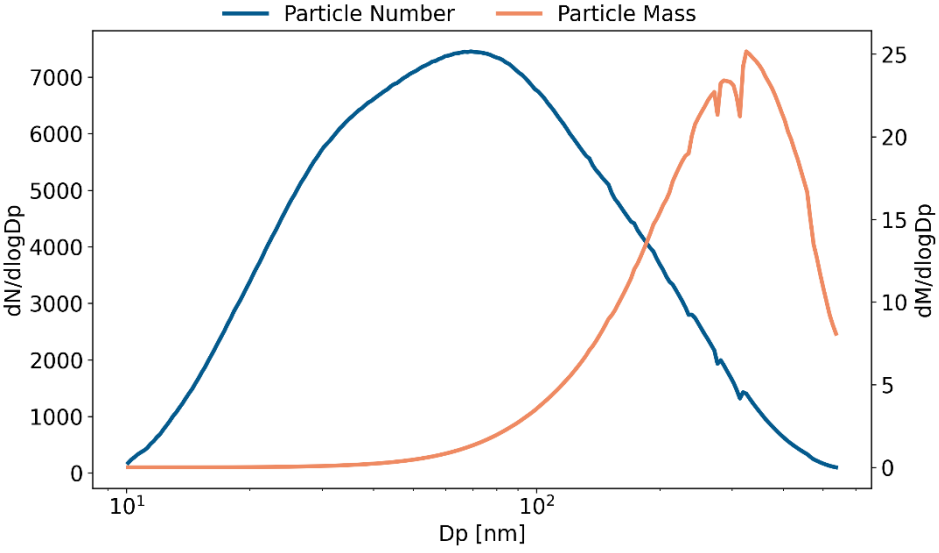

Figure S6: SMPS measurements from SKI between 28 September and 04 October 2023. Shown are the particle number dN/dlogDp [1 cm^{-3}] in blue and particle mass dM/dlogDp [µg m^{-3}] in orange over the measured size range [nm].

65

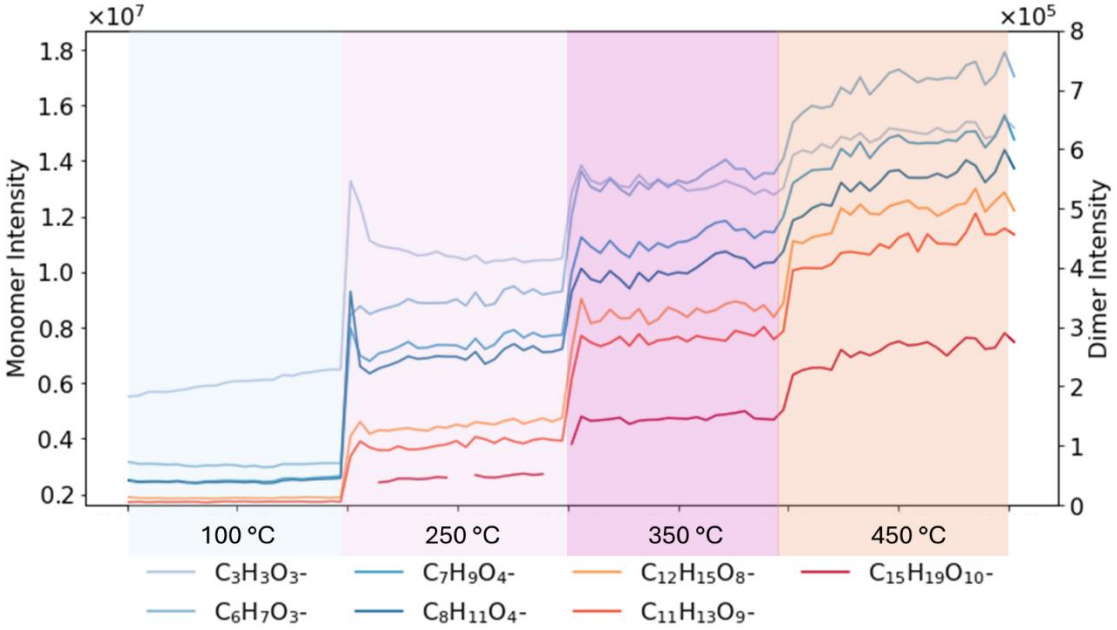

Figure S7: Vaporizer temperature stepping experiments from 100 °C, 250 °C, 350 °C to 450 °C for monomers intensity on the left-hand y-axis in and dimers intensity on the right-hand y-axis.

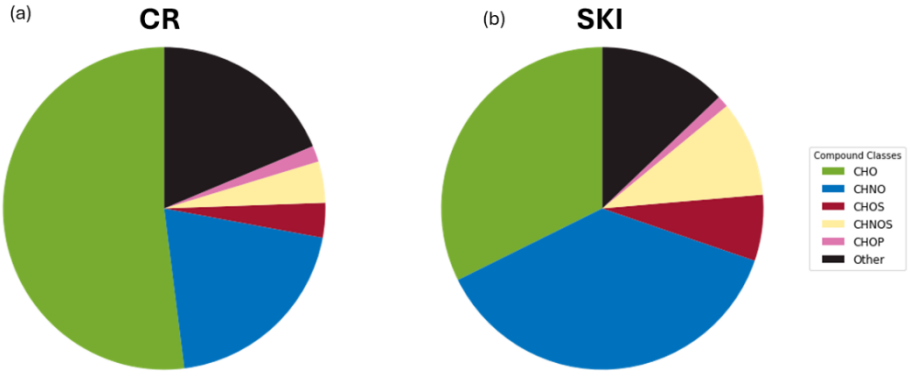

Figure S8: Attribution of molecular formulas from negative ionization mode to different compound classes which CHO (green), CHNO (blue), CHOS (red), CHNOS (yellow), CHOP (pink) and other compounds (black) for (a) CR and (B) SKI.

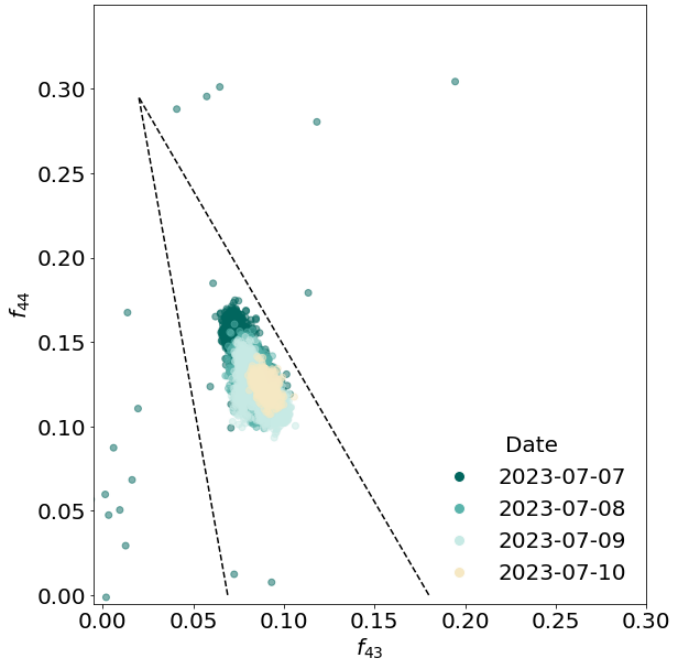

Figure S9: Triangle plot (*f*44 vs. *f*43) for CR between 07 July and 10. July 2023. The dotted lines are derived from Ng et al., (2010) indicating the area in which typical OOA lies.

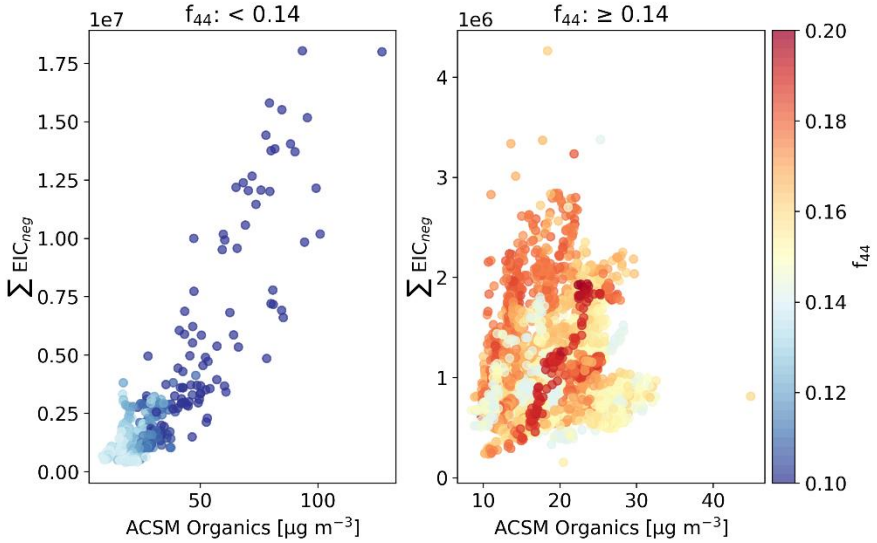

Figure S10: Pearson correlation of $\sum EIC_{neg}$ and ACSM organics species in SKI, colored by their respective f_{44} values. For better visualization separated f_{44} < 0.14 on the left and f $f_{44} \geq$ 0.14 on the right.

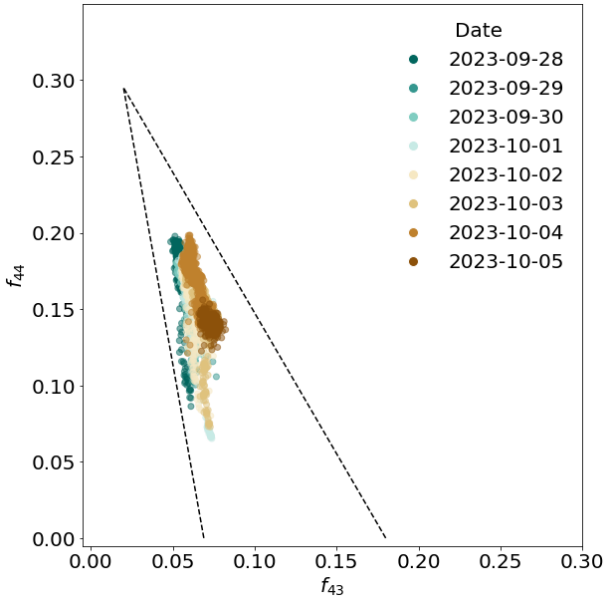

Figure S11: Triangle plot (f44 vs. f43) for SKI between 28. September and 04. October 2023. The dotted lines are derived from Ng et al. (2010) indicating the area in which typical OOA lies.

Table S1: Spectra data from negative ionization mode measurements recorded in SKI on the 28 September 2023 during a BB-event. Shown are the detected peaks from *m/z* 161 to 161.09, with information about the measured peak mass, the theoretical mass, the unambiguous attributed formula, the peak intensity, the ring and double-bond (RDB) equivalents and mass deviation in delta ppm.

Peak Mass	Theo. mass	Displayed Formula $[M-H]^-$	Intensity	RDB	Delta [ppm]
161.0092	161.00916	$C_5H_5O_6$	1.09×10^4	3.5	-0.06
161.0092					
161.0243	161.02442	$C_9H_5O_3$	2.18×10^4	7.5	-0.19
161.0356	161.03565	$C_8H_5O_2N_2$	2.51×10^4	7.5	-0.05
161.0454	161.04555	$C_6H_9O_5$	1.83×10^5	2.5	-0.27
161.0608	161.0608	$C_{10}H_9O_2$	1.51×10^4	6.5	-0.07
161.0721	161.07204	$C_9H_9ON_2$	4.77×10^3	6.5	-0.02
161.0819	161.08193	$C_7H_{13}O_4$	2.98×10^3	1.5	-0.17

Table S2: Spectra data from positive ionization mode measurements recorded in SKI on the 05 October 2023 during a BB-event. Shown are the detected peaks from *m/z* 163.02 to 163.135, with information about the measured peak mass, the theoretical mass, the unambiguous attributed formula, the peak intensity, the ring and double-bond (RDB) equivalents and mass deviation in delta ppm.

Peak Mass	Theo. mass	Displayed Formula $[M+H]^+$	Intensity	RDB	Delta [ppm]
163.0236	163.02371	$C_5H_7O_6$	1.16×10^4	2.5	0.55
163.0389	163.03897	$C_9H_7O_3$	1.43×10^5	6.5	0.38
163.0502	163.0502	$C_8H_7O_2N_2$	1.18×10^5	6.5	0.26
163.0602	163.0601	$C_6H_{11}O_5$	1.25×10^5	1.5	0.31
163.0755	163.07536	$C_{10}H_{11}O_2$	5.08×10^5	5.5	0.32
163.0867	163.08659	$C_9H_{11}ON_2$	2.18×10^5	5.5	0.31
163.0948			1.28×10^5		
163.0980			7.91×10^3		
163.1061			8.56×10^3		
163.1117	163.11174	$C_{11}H_{15}O$	$5.22E \times 10^4$	4.5	0.65
163.1140					
163.1230	163.12298	$C_{10}H_{15}N_2$	3.74×10^4	4.5	0.16
163.1330	163.13287	$C_8H_{19}O_3$	6.67×10^4	-0.5	0.48

85

Table S3: Instrumental sensitivity experiments with different reference standards and their respective concentration in standard solution [ug L−1], average signal background intensity, average signal intensity and produced mass concentration [µg m−3] used for normalization of Fig. 7

Compound	Polarity	Concentration in standard solution [ug L^{-1}]	Average signal background intensity	Average signal intensity	Produced particle mass concentration [µg m^{-3}]
MBTCA	$[M-H]^-$	5.11	1.55×10^5	9.11×10^7	35.43
MBTCA	$[M+H]^+$	5.11	1.69×10^4	8.03×10^6	35.43
Pinic Acid	$[M-H]^-$	2.4	1.22×10^6	1.17×10^7	1.77
Pinic Acid	$[M+H]^+$	2.4	1.72×10^5	2.95×10^6	1.77
Levoglucosan	$[M-H]^-$	1.2	1.85×10^5	3.02×10^6	0.44
Levoglucosan	$[M+H]^+$	1.2	1.74×10^3	3.91×10^4	0.42
Vanillin	$[M-H]^-$	116	7.99×10^5	2.69×10^6	2.23
Vanillin	$[M+H]^+$	116	3.56×10^4	4.48×10^5	2.22
Nitrocatechol	$[M-H]^-$	3.2	2.18×10^6	2.87×10^7	0.60
Nitrocatechol	$[M+H]^+$	3.2	1.12×10^3	1.12×10^5	0.72
Camphorsulfonic acid	$[M-H]^-$	3.3	0	7.70×10^7	4.28
Camphorsulfonic acid	$[M+H]^+$	3.3	9.19×10^3	3.37×10^6	4.26
Glyphosate	$[M-H]^-$	3.5	0	1.06×10^5	52.37
Glyphosate	$[M+H]^+$	3.5	0	1.20×10^4	52.37
Acridin	$[M+H]^+$	1.6	0	8.06×10^3	0.09
$C_{21}H_{23}O_4P$	$[M+H]^+$	2.1	0	2.44×10^6	20.86
$C_{29}H_{53}O_8$	$[M+H]^+$	2.1	0	4.28×10^5	20.86

.

Table S4: Chemical formulas attributed to OA in SKI and respective intensities for each compound class in negative $[M-H]^-$ and positive ionization mode $[M+H]^+$.

Compound class	∑Intensity	∑Attributed formulas
CHO $[M-H]^-$	9.22×10^9	1112
CHO $[M+H]^+$	4.84×10^9	1115
CHON $[M-H]^-$	2.22×10^9	1287
CHON $[M+H]^+$	4.82×10^9	1269
CHOS $[M-H]^-$	1.25×10^8	228
CHOS $[M+H]^+$	1.41×10^7	51
CHNOS $[M-H]^-$	8.25×10^7	330
CHNOS $[M+H]^+$	1.60×10^7	85
CHN $[M+H]^+$	4.34×10^8	155
Other $[M-H]^-$	1.18×10^9	443
Other $[M+H]^+$	7.90×10^7	511

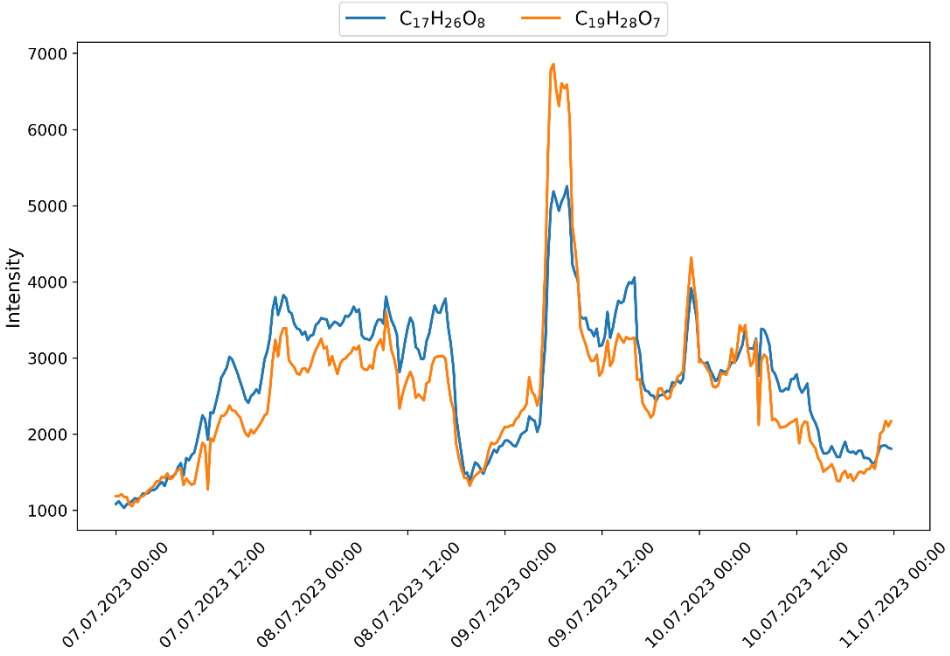

Figure S12: 30 minutes average intensity of $C_{17}H_{26}O_8$ (blue) and $C_{19}H_{28}O_7$ (orange) during ambient measurements at CR between 07 July and 10 July 2023.

References

Ng, N. L., Canagaratna, M. R., Zhang, Q., Jimenez, J. L., Tian, J., Ulbrich, I. M., Kroll, J. H., Docherty, K. S., Chhabra, P. S., Bahreini, R., Murphy, S. M., Seinfeld, J. H., Hildebrandt, L., Donahue, N. M., DeCarlo, P. F., Lanz, V. A., Prévôt, A. S. H., Dinar, E., Rudich, Y., and Worsnop, D. R.: Organic aerosol components observed in Northern Hemispheric datasets from Aerosol Mass Spectrometry, Atmos. Chem. Phys., 10, 4625–4641, https://doi.org/10.5194/acp-10-4625-2010, 2010.